

Spin-resolved imaging and spectroscopy of individual molecules with sub-molecular spatial resolution

Jens Brede and Roland Wiesendanger

Organic materials are fascinating and promising candidates for nanoscale spintronic devices and may open viable routes toward quantum computing. Previous experiments on spin transport in organic devices, through break junctions or spin valves, unveiled exciting new frontiers of molecular magnetism. However, much more effort is needed to understand the properties of organic/magnetic interfaces at a microscopic level. In this article, we show how spin-polarized scanning tunneling microscopy and spectroscopy (SP-STM/STS) can provide unprecedented insights into organic/magnetic interfaces as an initial step toward favorably tailoring such interfaces in order to increase device efficiency. Based on the unique combination of spin-sensitivity, atomic-scale spatial resolution, and high-energy resolution, SP-STM/STS has proven to be an invaluable method for exploring spatial and bias dependences of spin-polarized currents through individual molecules as well as for revealing individual spin-split molecular orbitals interacting with ferromagnetic substrates.

Introduction: Molecular electronics

Component miniaturization in the semiconductor industry has been remarkable and has even outperformed the ambitious predictions put forth by Moore's law, which states that the number of transistors per integrated circuit doubles every two years. Molecular electronics stems from the idea of performing the basic functions of electronics—rectification, amplification, and storage—with few or even single molecules embedded between electrodes.¹ Indeed, rapid progress in both the understanding and experimental realization of molecular devices has been achieved.² In optoelectronics, organic light-emitting diodes as well as organic photovoltaics have found their way into the marketplace and are competing with conventional semiconductor technology today. Nonetheless, inorganic semiconductor electronics is the current benchmark: transistors available in the market are as small as 22 nm, and a reduction down to 5 nm is technologically within reach already. These are dimensions that are comparable to many single molecules that were envisioned to replace their inorganic counterparts, provoking the question of whether the original promise of organic molecular electronics can still be fulfilled.

Molecule-based devices show potential in a new field within electronics that not only uses the charge of the electron but also uses its spin (e.g., to store data or perform computations).

The area of research that addresses the question of how spins can be injected, manipulated, and detected in the solid state is collectively referred to as spintronics (see the Introductory article in this issue). Recent pioneering experiments and theoretical studies suggest that organic materials can offer similar or even superior performance in spin-based devices compared to their inorganic metallic or semiconducting counterparts.³ Experiments on spin transport through break junctions⁴ and spin valves^{5,6} (see the article by Nguyen et al. in this issue) have unveiled exciting new frontiers of molecular magnetism. In particular, single molecule magnets are, if deposited on appropriate electrodes, a viable route toward quantum computing.^{7–9} However, in order to understand the processes determining the spin-dependent characteristics of organic systems in contact with a ferromagnetic (FM) electrode, microscopic insights into interface properties, including information on the local spin-resolved transport through single molecules, is required. Spin-polarized scanning tunneling microscopy (SP-STM) is a tool that can address these fundamental issues.¹⁰

Local spin-resolved experiments on single molecules on surfaces

Experiments on organic semiconductors (OSCs) have revealed substantial spin relaxation times and significant spin diffusion

Jens Brede, Institute of Applied Physics and Interdisciplinary Nanoscience Center Hamburg, University of Hamburg, Germany; jbrede@physnet.uni-hamburg.de
Roland Wiesendanger, Department of Physics, University of Hamburg, Germany; wiesendanger@physnet.uni-hamburg.de
DOI: 10.1557/mrs.2014.127

lengths of spin-polarized carriers.^{11–15} These observations are attributed to the weak spin-orbit coupling typical for organic materials composed of light elements such as C and H. Intensive research efforts started when spin-polarized transport—characterized by giant magnetoresistance (MR)—was demonstrated in organic spin valves (OSVs) in the first years of the new millennium.^{11,12} Many additional experiments using various OSVs have since been performed in an attempt to prove spin-injection as well as transport through OSCs (**Figure 1a**).

The vast majority of these studies were performed using spatially averaging techniques in device set-ups where the microscopic composition of the OSV remained (at least partially) unknown. Many material-related problems—schematically depicted in **Figure 1c** for a “real” OSV—were encountered: interdiffusion of magnetic atoms from one of the electrodes into the OSC, the existence of defects and impurities, as well as interface roughness between the FM electrodes and the OSC. More general, a strong deviation of the properties known for bulk-like OSC can be expected at the interfaces with FM electrodes.¹⁵

SP-STM offers a microscopic solution to many of these problems. The principle of the set-up is similar to that for a planar OSV, but all experiments are typically performed under ultrahigh vacuum conditions. This allows the preparation of an atomically flat FM-sample electrode (e.g., a two atomic layer thick FM Fe-film grown on a W(110) surface that is probed with an *in situ* Fe-coated W-tip, see **Figure 1b**). Both tip and sample systems were extensively characterized by means of SP-STM.¹⁰ Note that FM electrodes of planar OSVs typically exhibit an in-plane magnetization direction, while the SP-STM-derived OSV discussed here exhibits out-of-plane magnetization directions of tip and sample electrodes. Isolated molecules can be deposited on top of the FM-sample electrode *in situ* by thermal evaporation of thoroughly outgassed organic material (e.g., phthalocyanine (Pc) molecules). The as-prepared Fe-film exhibits a magnetic domain structure with alternating parallel (⊙) and antiparallel (⊗) magnetized domains, respectively (i.e., the magnetization direction of the sample is collinear with the surface normal and locally either parallel or antiparallel with respect to the tip magnetization direction).

Due to the alternating magnetic domains, a comparison between molecules adsorbed on oppositely magnetized domains^{16–21} can be used to calculate the MR, or—when equipped with an external magnetic field (B_{ext})—a traditional spin-valve experiment can be performed by reversing the magnetization of one of the FM electrodes (e.g., the FM tip) by application of B_{ext} and subsequently measuring the same molecule with parallel and antiparallel configuration of the two FM electrodes, respectively.^{22–24} The result of a magnetization reversal of the FM tip electrode is illustrated in **Figure 1d**: the magnetic contrast of the FM sample electrode is inverted (i.e., the sample domains that were first parallel (⊙)/antiparallel (⊗) with respect to the tip magnetization direction are now antiparallel (⊗)/parallel (⊙), respectively).

Spin- and energy-resolved tunneling with submolecular resolution

SP-STM offers atomic-scale control of the OSV junction. Moreover, it allows probing spin-dependent transport through a single molecule with submolecular spatial and high energy resolution. The SP-STM images presented in **Figure 1d** and **Figure 2** were recorded in constant-current mode at the set-current I and sample bias voltage V . In this case, the local effective polarization (P) of the atomic-scale tunnel junction can directly be determined from height variations Δs resulting from oppositely magnetized domains, as introduced by Wiesendanger et al.²⁵

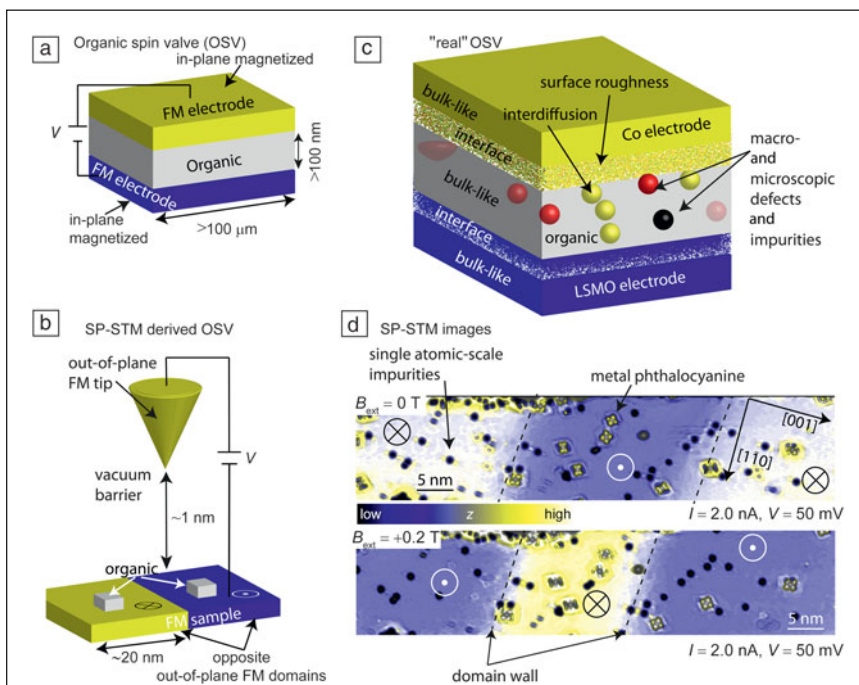
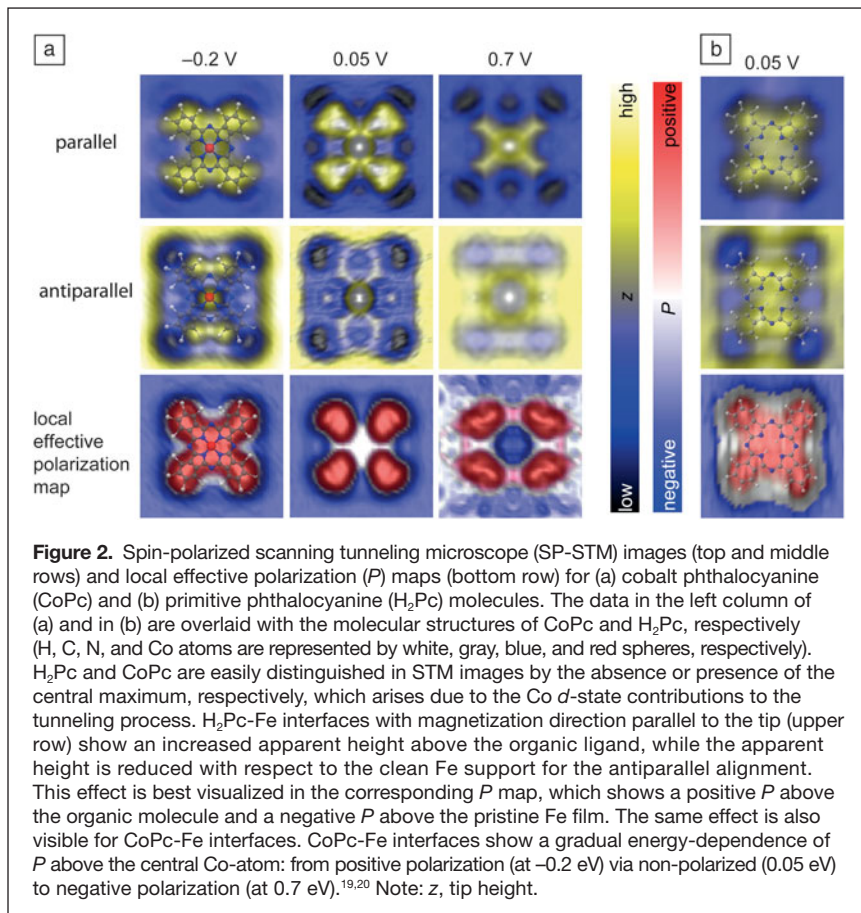


Figure 1. Schematic comparison of (a) a planar organic spin valve (OSV) and (b) a spin-polarized scanning tunneling microscopy (SP-STM)-derived OSV. (c) A “real” OSV suffers from problems such as interdiffusion or metallic inclusions, defects, and impurities, as well as interface roughness (adapted from Reference 15). In contrast, a SP-STM-derived OSV is prepared in an ultrahigh vacuum with subnanometer control of the ferromagnetic (FM) organic interfaces. Typically, the FM sample, here, two atomic layers of Fe grown on W(110), exhibits alternating parallel (⊙) and antiparallel (⊗) domain structures that lead to a subtle variation of the tip height (z) from blue (low) to yellow (high) in (d) SP-STM images. Phthalocyanine molecules, exhibiting a clover leaf shape in the SP-STM images, are found on both magnetic domains and are easily distinguished from other atomic-scale species (circular features). The alternating domain structure allows local measurements of the transport in the parallel and antiparallel spin valve geometry on the same sample. Alternatively, an external magnetic field (B_{ext}) can be applied to control the magnetization direction of the tip (or the sample). Reversing the magnetization direction of the tip leads to an inversion of the magnetic contrast of the sample.¹⁹ Note: LSMO, $\text{La}_{0.67}\text{Sr}_{0.33}\text{MnO}_3$; I , tunneling current; V , applied bias voltage.



$$P = \frac{e^{a\sqrt{\phi}\Delta s} - 1}{e^{a\sqrt{\phi}\Delta s} + 1} = \tanh\left(\frac{a}{2}\sqrt{\phi}\Delta s\right) \approx \frac{\Delta s < 1\text{\AA}}{a/2\sqrt{\phi}\Delta s}, \quad (1)$$

where ϕ denotes the mean local tunneling barrier height and $a \cong 1 \text{ eV}^{-1/2} \text{\AA}^{-1}$.

The continuous color variation of the Fe film from blue to yellow in the SP-STM images shown in Figure 1d between opposite magnetic domains corresponds to Δs of a few up to tens of picometers, depending on the details of the tunneling barrier. The spin-dependent transport from the FM sample through the molecules to the FM tip is conveniently visualized by calculating the difference between data obtained for molecules with identical adsorption geometries but on oppositely magnetized domains (Figure 2). The so-called local effective polarization maps reveal two striking features: (1) an inversion of P on the organic ligand (red = positive P) compared to the Fe-substrate (blue = negative P), which is visible in a broad energy interval and independent of the presence of the central molecular cobalt atom (as is evident by comparison of CoPc with the metal-free H_2Pc in Figure 2); (2) an energy-dependent P of the central Co-ion.

When tunneling out of the occupied states (at $V = -0.2$ V), the spin-polarized current originating from the cobalt atom has positive P , while for tunneling into the states close to the

Fermi level ($V = 0.05$ V), P is zero at the Co-site (as evident by the white area in the corresponding P -map). When increasing the bias voltage ($V = +0.7$ V), transport through the central Co-atom is predominantly of negative polarization (clearly shown by the blue coloring in the corresponding P -map). The gradual change in P above the central Co-ion of CoPc molecules on an Fe electrode is a direct consequence of the strong hybridization of molecular orbitals and substrate states.²⁰ The spin-resolved data not only provide precise experimental information on how and where a molecule needs to be contacted to achieve, for a given bias voltage applied, the desired spin-filtering effect (e.g., on the organic ligand or the central metal atom), but also provide the surprising observation of the inversion of P on the organic ligand with respect to the FM Fe film. This effect was already postulated by density functional theory (see the article by Atodiresei et al. in this issue) for CoPc molecules on a FM cobalt film¹⁶ and since then experimentally verified for a variety of Pc molecules on different FM films^{19,20,23} as well as for three-dimensional molecules such as C_{60} ,¹⁷ $TbPc_2$,²² or zinc-methyl-phenalenyl.²⁶

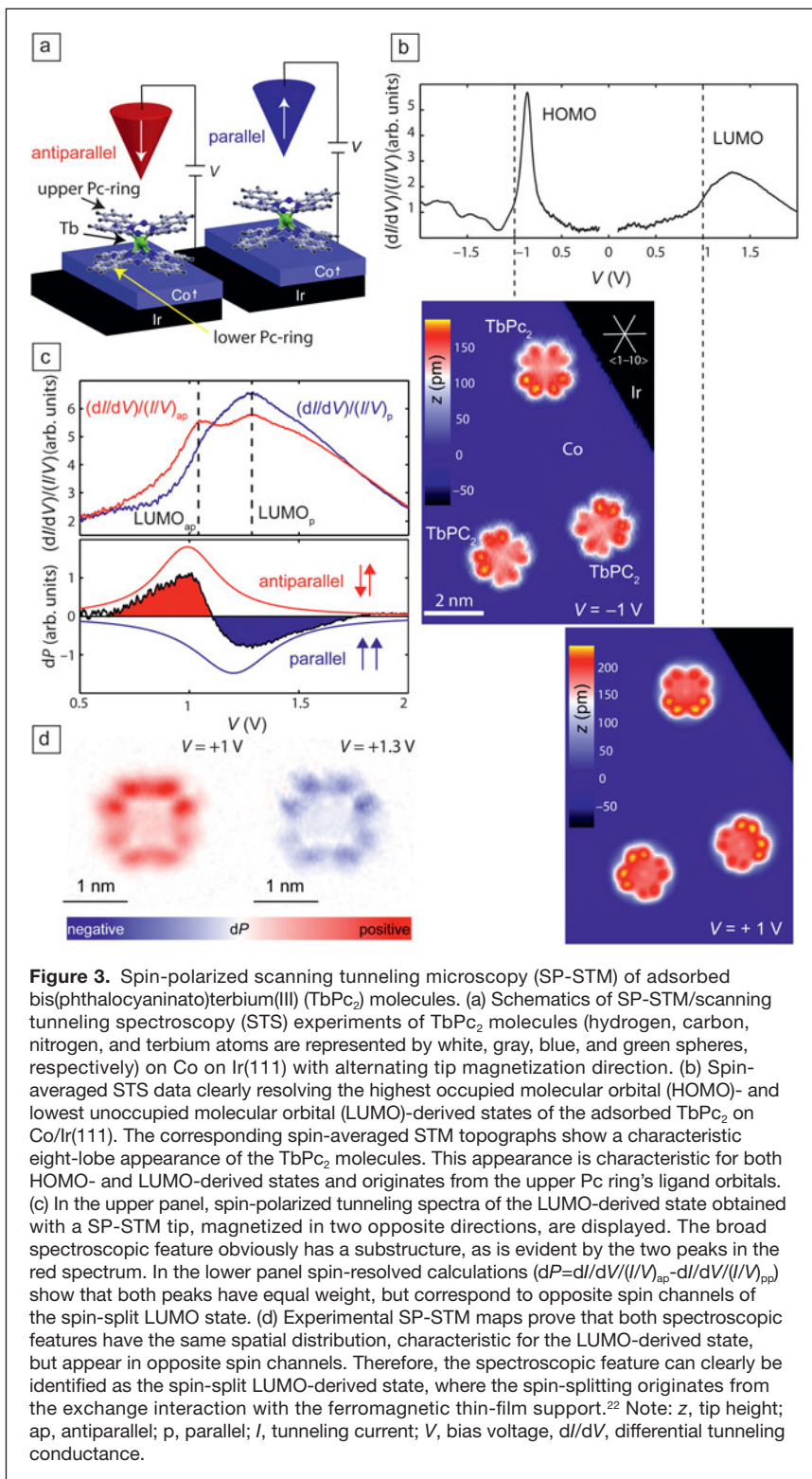
These experimental observations had a significant impact on the interpretation of results on the OSV because they offered an explanation for the puzzling and strongly debated

negative MR in such structures. Indeed, in parallel with spin-resolved scanning probe studies, a local solid-state device experiment and an x-ray absorption spectroscopy investigation led to similar conclusions.^{27,28}

Real-space observations of spin-split molecular orbitals of adsorbed single-molecule magnets

Single-molecule magnets (SMMs) exhibit a variety of fascinating properties, such as hysteresis,²⁹ slow relaxation³⁰ and quantum tunneling of magnetization,^{30,31} tunable coupling to magnetic substrates,^{32,33} and electric control of molecular spin states.³⁴ Recently, the realization of novel devices, such as multiple-field-effect nanotransistors³⁵ or supramolecular spin valves,³⁶ was reported, demonstrating the potential of SMMs for technological applications, in particular spintronics and quantum computing. Further progress in the field requires a detailed understanding of structural and electronic properties, as well as magnetic interactions of individual SMMs in contact with a FM electrode in an atomically well-defined environment.

In many previous studies, bis(phthalocyaninato)terbium(III) ($TbPc_2$, see Figure 3a) was chosen as a model-type system because of its high blocking temperature ($T_B \sim 30$ – 50 K, where the blocking temperature is the temperature below which a superparamagnetic particle remains “blocked” in the same (initial) state during the time of measurement),^{37,38} its comparably



small size, and its high stability, which allows for thermal deposition of the molecules onto FM substrates in ultrahigh vacuum (UHV).³⁹

The electronic structure of TbPc_2 adsorbed on an ultrathin Co film deposited on Ir(111) has been investigated by local

tunneling spectroscopy above a single molecule.²² The spin-averaged normalized differential tunneling conductance ($dI/dV)/(I/V)$ as a function of the applied bias voltage V (Figure 3b) shows two pronounced peaks at $V = -0.9$ V and $V = +1.3$ V. These spectroscopic features can be attributed to the highest occupied molecular orbital (HOMO)- and lowest unoccupied molecular orbital (LUMO)-derived states of the molecule, respectively, hybridized with the substrate states, leading to spectroscopic broadening. The spatial distribution of these states is imaged in the respective topographs (below) and shows an eight-lobe structure for both HOMO- and LUMO-derived states. This particular appearance is characteristic for π -orbitals of phthalocyanine molecules only weakly interacting with the surface. The observation of a similar eight-lobe structure for the TbPc_2 molecules indicates that primarily the upper Pc ring is imaged, and it is only weakly electronically interacting with the Co-film support. The appearance of an eight-lobe structure is expected for both a neutral $[\text{TbPc}_2]^0$ (with the ligand spin still present) as well as for a negatively charged $[\text{TbPc}_2]^-$ molecule (with the ligand spin quenched by charge transfer from the substrate).^{39,40} Therefore, spin-averaged STS measurements cannot distinguish between the charged and the neutral states of adsorbed TbPc_2 molecules. Moreover, spin-averaged measurements cannot directly determine the spin state of the frontier orbitals. In order to address the spin character of these orbitals, SP-STM/STS data have to be collected.

Measuring the energy dependence of the LUMO-derived state with a spin-polarized tip for parallel and antiparallel tip and sample magnetization directions (Figure 3c) shows that two states of opposite spin character are in the energy range spanned by the broad LUMO-derived feature in spin-averaged data. Moreover, the spin-resolved local tunneling spectroscopy data show that the broad feature with a maximum at $V = +1.3$ V, which was assigned to the LUMO-derived state in the spin-averaged spectrum (Figure 3b), in fact contains two spectroscopic features: a first peak at $V = +1.1$ V being clearly visible only if tip and sample magnetizations are aligned antiparallel (referred to as LUMO_{ap} in the following), while the second peak at $V = +1.2$ V is more pronounced if tip and sample magnetizations are aligned parallel (LUMO_{p}). The lower panel of Figure 3c depicts the difference of the spin-resolved normalized differential tunneling conductance for

antiparallel and parallel alignment (dP), which is a measure of the spin polarization of the LUMO-derived state. Clearly, the two parts of the LUMO-derived state are of opposite spin character. Their exact energetic positions are determined by fitting two Lorentzian functions. The areas below the “antiparallel” and the “parallel” LUMO features are equal, indicating that the total spin polarization of the entire LUMO-derived state is zero.

After determining the spin character of the states, as observed in local tunneling spectroscopy, the spatial distributions of these states were mapped by constant-height SP-STM measurements. In order to avoid any topographic effects in SP-STM data, the tip was stabilized above the non-magnetic Ir substrate, which resulted in the same tip-sample distance for both parallel and antiparallel alignment of the SP-STM tip and Co-film magnetization directions. The difference between the antiparallel and parallel cases yields information about the spatial distribution of the molecular spin polarization at a given energy (Figure 3d): For $V = +1.0$ V, it is positive, while it is negative for $V = +1.3$ V, consistent with the local tunneling spectroscopy data. More importantly, both SP-STM maps at $V = +1.0$ V and $V = +1.3$ V clearly reveal the same eight lobe orbital structure. The fact that an identical spatial distribution with opposite spin character is observed allows an unambiguous attribution of the two spectral features in the different spin channels to the same molecular orbital (i.e., spatially and energetically the spin splitting of the LUMO-derived π -orbital state is resolved). The magnitude of the spin splitting of the LUMO-derived state amounts to $\Delta E = eV_{\text{LUMO}p} - eV_{\text{LUMO}ap} = 210 \pm 20$ meV (e denotes the elementary charge of the electron), whereas the total spin polarization of the LUMO-derived state is zero, as already mentioned, thereby excluding the presence of an unpaired electron in the LUMO-derived state. The value ΔE of ~ 210 meV determined for the spin splitting is comparable to the ~ 500 meV observed for C_{60} in contact with a Fe film.¹⁷

Interestingly, the spin-resolved STM data allow an unambiguous determination of the charge state of the TbPc₂ molecule: the isolated TbPc₂ molecule has an unpaired spin on the organic ligand; this radical would show up in an SP-STM experiment as a spectroscopic feature for both bias polarities (i.e., below and above the Fermi energy). A spin-dependent spatial mapping of these features would show the same molecular orbital, but with opposite spin character, similar to the situation observed in our experiment, however, at opposite bias polarities. The fact that we observed this behavior only for the positive bias polarity means that the orbital is completely empty, and therefore the radical spin must be quenched upon adsorption of the TbPc₂ molecule on the Co-film.

Summary

Spin-polarized scanning tunneling microscopy/scanning tunneling spectroscopy (SP-STM/STS) studies of individual CoPc (Pc = phthalocyanine) molecules adsorbed on a ferromagnetic (FM) Fe thin film were presented, revealing the

energy-dependent spin transport through a single molecule with intramolecular spatial resolution. The current flowing through the adsorbed CoPc molecule shows a high, spatially varying spin polarization ranging from inversion up to amplification with respect to the FM Fe film, depending on the particular functional unit of the molecule (i.e., metal-ion site or organic ligand). The observed spatial dependence of the spin-polarized current flowing through the molecule is identified as a result of the formation of molecule-substrate hybrid states by a combined SP-STM and density functional theory approach. In particular, the π - d hybridization present for organic molecules chemisorbed on magnetic surfaces has since been observed for a variety of systems and led to the discovery of novel effects such as magnetic hardening of thin films by adsorption of organic molecules. In the future, fundamentally new aspects of organic spintronics can be expected to be unveiled by SP-STM/STS when organic molecules are studied on more complex magnetic surfaces, such as antiferromagnets, non-collinear spin-states, and skyrmionic lattices.

SP-STM/STS investigations of adsorbed TbPc₂ molecules have led to an unambiguous experimental determination of their charge and spin state: the radical spin was found to be quenched upon adsorption of the TbPc₂ molecule on a Co film support, as in the case of adsorbed CoPc molecules on ultrathin Fe films. These central experimental observations are of crucial importance for potential device applications of TbPc₂, as the coupling of the Tb-ion to its surrounding is believed to be mediated by the ligand orbitals. Key challenges in the field remain in accessing and manipulating the f -states of, for example, the Tb-ion directly with SP-STM or addressing individual spin-centers in single-molecule magnets (SMMs) such as manganese-12-acetate. Furthermore, pushing the temporal resolution in SP-STS below the nanosecond regime will open a viable route toward studying and controlling the processes of magnetization reversal in SMMs and organic-ferromagnetic hybrids in atomically well-defined environments with sub-molecular precision.

Acknowledgments

We would like to thank all our collaborators, in particular N. Atodiresei, S. Blügel, V. Caciuc, A. Dilullo, Y.-S. Fu, G. Hoffmann, S. Klyatskaya, P. Lazic, M.-H. Prosenc, M. Ruben, and J. Schwöbel for their contributions. Financial support from the ERC Advanced Grant FUIRORE and by the Deutsche Forschungsgemeinschaft via the SFB 668 is gratefully acknowledged.

References

1. A. Aviram, M.A. Ratner, *Chem. Phys. Lett.* **29**, 277 (1974).
2. C. Joachim, J. Gimzewski, A. Aviram, *Nature* **408**, 541 (2000).
3. S. Sanvito, *Chem. Soc. Rev.* **40**, 3336 (2011).
4. L. Bogani, W. Wernsdorfer, *Nat. Mater.* **7**, 179 (2008).
5. V.A. Dediu, L.E. Hueso, I. Bergenti, C. Taliani, *Nat. Mater.* **8**, 707 (2009).
6. J.-W. Yoo, C.-Y. Chen, H.W. Jang, C.W. Bark, V.N. Prigodin, C.B. Eom, A.J. Epstein, *Nat. Mater.* **9**, 638 (2010).
7. M.N. Leuenberger, D. Loss, *Nature* **410**, 789 (2001).
8. A. Dei, D. Gatteschi, *Angew. Chem. Int. Ed.* **50**, 11852 (2011).

9. M. Warner, S. Din, I.S. Tupitsyn, G.W. Morley, A.M. Stoneham, J.A. Gardener, Z. Wu, A.J. Fisher, S. Heutz, C.W.M. Kay, G. Aeppli, *Nature* **503**, 504 (2013).
10. R. Wiesendanger, *Rev. Mod. Phys.* **81**, 1495 (2009).
11. V. Dediu, M. Murgia, F.C. Matocota, C. Taliani, S. Barbanera, *Solid State Commun.* **122**, 181 (2002).
12. Z.H. Xiong, D. Wu, Z. Vally Vardeny, J. Shi, *Nature* **427**, 821 (2004).
13. A.J. Drew, J. Hoppler, L. Schulz, F.L. Pratt, P. Desai, P. Shakya, T. Kreouzis, W.P. Gillin, A. Suter, N.A. Morley, V.K. Malik, A. Dubroka, K.W. Kim, H. Bouyanfif, F. Bourqui, C. Bernhard, R. Scheuermann, G.J. Nieuwenhuys, T. Prokscha, E. Morenzoni, *Nat. Mater.* **8**, 109 (2009).
14. M. Cinchetti, K. Heimer, J.-P. Wustenberg, O. Andreyev, M. Bauer, S. Lach, C. Ziegler, Y. Gao, M. Aeschlimann, *Nat. Mater.* **8**, 115 (2009).
15. D. Sun, E. Ehrenfreund, Z.V. Vardeny, *Chem. Commun.* **50**, 1781 (2014).
16. C. Iacovita, M.V. Rastei, B.W. Heinrich, T. Brumme, J. Kortus, L. Limot, J.P. Bucher, *Phys. Rev. Lett.* **101**, 116602 (2009).
17. S.L. Kawahara, J. Lagoute, V. Repain, C. Chacon, Y. Girard, S. Rousset, A. Smogunov, C. Barreateau, *Nano Lett.* **12**, 4558 (2012).
18. T. Methfessel, S. Steil, N. Baadji, N. Großmann, K. Koffler, S. Sanvito, M. Aeschlimann, M. Cinchetti, H.J. Elmers, *Phys. Rev. B: Condens. Matter* **84**, 224403 (2011).
19. J. Brede, N. Atodiresei, S. Kuck, P. Lazić, V. Caciuc, Y. Morikawa, G. Hoffmann, S. Blügel, R. Wiesendanger, *Phys. Rev. Lett.* **105**, 047204 (2010).
20. N. Atodiresei, J. Brede, P. Lazić, V. Caciuc, G. Hoffmann, S. Blügel, R. Wiesendanger, *Phys. Rev. Lett.* **105**, 066601 (2010).
21. M. Garnica, D. Stradi, S. Barja, F. Calleja, C. Díaz, M. Alcami, N. Martín, A.L. Vázquez de Parga, F. Martín, R. Miranda, *Nat. Phys.* **9**, 368 (2013).
22. J. Schwöbel, Y. Fu, J. Brede, A. Dillullo, G. Hoffmann, S. Klyatskaya, M. Ruben, R. Wiesendanger, *Nat. Commun.* **3**, 953 (2012).
23. J. Brede, R. Wiesendanger, *Phys. Rev. B: Condens. Matter* **86**, 184423 (2012).
24. Y.-S. Fu, Q.-K. Xue, R. Wiesendanger, *Phys. Rev. Lett.* **108**, 087203 (2012).
25. R. Wiesendanger, H.-J. Güntherodt, G. Güntherodt, R.J. Gambino, R. Ruf, *Phys. Rev. Lett.* **65**, 247 (1990).
26. K.V. Raman, A.M. Kamerbeek, A. Mukherjee, N. Atodiresei, T.K. Sen, P. Lazić, V. Caciuc, R. Michel, D. Stalke, S.K. Mandal, S. Blügel, M. Münzenberg, J.S. Moos, *Nature* **493**, 509 (2013).
27. C. Barraud, P. Seneor, R. Mattana, S. Fusil, K. Bouzehouane, C. Deranlot, P. Graziosi, L. Hueso, I. Bergenti, V. Dediu, F. Petroff, A. Fert, *Nat. Phys.* **6**, 615 (2010).
28. S. Javaid, M. Bowen, S. Boukari, L. Joly, J.-B. Beaufrand, X. Chen, Y.J. Dappe, F. Scheurer, J.-P. Kappler, J. Arabski, W. Wulfhekel, M. Alouani, E. Beaupaire, *Phys. Rev. Lett.* **105**, 077201 (2010).
29. M. Mannini, F. Pineider, P. Sainctavit, C. Danieli, E. Otero, C. Sciancalepore, A.M. Talarico, M.-A. Arrio, A. Cornia, D. Gatteschi, R. Sessoli, *Nat. Mater.* **8**, 194 (2009).
30. R. Sessoli, D. Gatteschi, A. Caneschi, M.A. Novak, *Nature* **365**, 141 (1993).
31. N. Ishikawa, M. Sugita, W. Wernsdorfer, *Angew. Chem. Int. Ed.* **44**, 2931 (2005).
32. A.L. Rizzini, C. Krull, T. Balashov, J.J. Kavich, A. Mugarza, P.S. Miedema, P.K. Thakur, V. Sessi, S. Klyatskaya, M. Ruben, S. Stepanow, P. Gambardella, *Phys. Rev. Lett.* **107**, 177205 (2011).
33. L. Malavolti, L. Poggini, L. Margheriti, D. Chiappe, P. Graziosi, B. Cortigiani, V. Lanzilotto, F. Buatier de Mongeot, P. Ohresser, E. Otero, F. Choueikani, P. Sainctavit, I. Bergenti, V.A. Dediu, M. Mannini, R. Sessoli, *Chem. Commun.* **49**, 11506 (2013).
34. J. Kanamori, K. Terakura, *J. Phys. Soc. Jpn.* **70**, 1433 (2002).
35. A. Candini, S. Klyatskaya, M. Ruben, W. Wernsdorfer, M. Affronte, *Nano Lett.* **11**, 2634 (2011).
36. M. Urdampilleta, S. Klyatskaya, J.-P. Cleuziou, M. Ruben, W. Wernsdorfer, *Nat. Mater.* **10**, 502 (2011).
37. N. Ishikawa, M. Sugita, T. Ishikawa, S. Koshihara, Y. Kaizu, *J. Am. Chem. Soc.* **125**, 8694 (2003).
38. F. Branzoli, P. Carretta, M. Filibian, G. Zoppellaro, M.J. Graf, J.R. Galan-Mascaros, O. Fuhr, S. Brink, M. Ruben, *J. Am. Chem. Soc.* **131**, 4387 (2009).
39. T. Komeda, H. Isshiki, J. Liu, Y.-F. Zhang, N. Lorente, K. Katoh, B.K. Breedlove, M. Yamashita, *Nat. Commun.* **2**, 217 (2011).
40. L. Vitali, S. Fabris, A.M. Conte, S. Brink, M. Ruben, S. Baroni, K. Kern, *Nano Lett.* **8**, 3364 (2008). □



8th International Workshop on Zinc Oxide and Related Materials

September 7-11, 2014 // Sheraton on the Falls Hotel
Niagara Falls, Ontario, Canada

PREREGISTER NOW AND SAVE!

Scientific Program

The five-day Conference will feature oral and poster presentations covering:

- Bulk crystal growth
- Homoepitaxial and heteroepitaxial thin film growth
- Alloys (e.g. ZnMgO, IGZO, ZnCdO, BaSnO₃, GIZO)
- Quantum confined structures
- Band structure
- Optical properties
- Surface and interface electronic properties
- Defect identification, control and modeling
- Doping and electrical properties
- Schottky junctions, contacts, transparent electrodes
- Ferromagnetic layers for spintronic devices
- Transistors, TFTs, high frequency electronics
- Optoelectronic devices
- Piezoelectric, acousto-optic, gas, chemical and biosensor device applications
- Polarization engineered device concepts

www.mrs.org/iwzno-2014